LETTER

doi:10.1038/nature10010

Single-ion quantum lock-in amplifier

Shlomi Kotler[1], Nitzan Akerman[1], Yinnon Glickman[1], Anna Keselman[1] & Roee Ozeri[1]

Quantum metrology[1] uses tools from quantum information science to improve measurement signal-to-noise ratios. The challenge is to increase sensitivity while reducing susceptibility to noise, tasks that are often in conflict. Lock-in measurement is a detection scheme designed to overcome this difficulty by spectrally separating signal from noise. Here we report on the implementation of a quantum analogue to the classical lock-in amplifier. All the lock-in operations—modulation, detection and mixing—are performed through the application of non-commuting quantum operators to the electronic spin state of a single, trapped Sr^+ ion. We significantly increase its sensitivity to external fields while extending phase coherence by three orders of magnitude, to more than one second. Using this technique, we measure frequency shifts with a sensitivity of 0.42 Hz $Hz^{-1/2}$ (corresponding to a magnetic field measurement sensitivity of 15 pT $Hz^{-1/2}$), obtaining an uncertainty of less than 10 mHz (350 fT) after 3,720 seconds of averaging. These sensitivities are limited by quantum projection noise and improve on other single-spin probe technologies[2,3] by two orders of magnitude. Our reported sensitivity is sufficient for the measurement of parity non-conservation[4], as well as the detection of the magnetic field of a single electronic spin one micrometre from an ion detector with nanometre resolution. As a first application, we perform light shift spectroscopy of a narrow optical quadrupole transition. Finally, we emphasize that the quantum lock-in technique is generic and can potentially enhance the sensitivity of any quantum sensor.

Quantum probes with unprecedented sensitivities are advancing the field of metrology. In particular, cold, trapped ions are well isolated from their environment and their internal states and motion can be controlled with high fidelity, thus enabling researchers to use them as excellent probes[5,6].

Achieving a high signal-to-noise ratio involves demands—decreasing the effect of noise on the probe while enhancing its response to the measured signal—that are often in conflict. The problem arises if the noise and the signal couple to the probe through the same physical channel. Quantum metrology uses methods from quantum coherent control to address this difficulty. As an example, entangled states that are invariant under certain noise mechanisms have been engineered with trapped ions and have demonstrated long coherence times[7–9]. Other entangled states have been similarly engineered to enhance the measurement sensitivity of trapped ions[10,11]. Whether or not the measurement signal-to-noise ratio improves depends on the commutativity of the noise and signal operators as well as on the noise bandwidth[12–14].

A different approach to noise reduction is based on spectrally separating a quantum system from its noise environment. Such time-dynamical noise decoupling has been demonstrated using trapped-ion quantum bits, among other systems, and has been optimized to match different noise profiles[15,16]. In fact, it was shown that the decoherence rate of these modulated systems can be used to extract information about their noise spectrum[16–18]. A natural extension to spectral characterization is the measurement of oscillating signals. Dynamical manipulation can therefore be used to decouple a quantum probe from noise while enhancing its sensitivity to alternating signals.

In the past few years, dynamical decoupling methods have been used to improve on the signal-to-noise ratio of a.c. magnetometry using nitrogen-vacancy centres[19–22]. Indeed, significant enhancement of sensitivity was achieved using a few tens of modulation pulses[22]. However, owing to the particular decoherence mechanism in nitrogen-vacancy centres, their best reported magnetic field measurement sensitivity, of 4 nT $Hz^{-1/2}$, was achieved using a single echo pulse[3].

In this work, we show that a quantum probe, time evolving under non-commuting noise, signal and modulation operators, is equivalent to a lock-in amplifier. We take full advantage of the quantum lock-in method, with up to 650 modulation pulses, using a single trapped $^{88}Sr^+$ ion. The lock-in method provides a 30-fold improvement in frequency-shift measurement sensitivity. We demonstrate a record sensitivity for a single-spin detector[2,3], of 15 pT $Hz^{-1/2}$ (0.42 Hz $Hz^{-1/2}$), reaching a measurement uncertainty of less than 10 mHz (350 fT) after 3,720 s of averaging.

Classical lock-in amplifiers are detectors that can extract a signal with a known carrier frequency from an extremely noisy environment. Schematically, if noise, $N(t)$, adds to a physical observable, S_0, oscillating at a frequency f_m, the total signal measured by the detector is $M(t) = m_0[S_0\cos(2\pi f_m t + \varphi) + N(t)]$. Here m_0 sets the detector measurement units and φ is a constant phase. A signal proportional to S_0 is obtained by a mix-down process: $M(t)$ is multiplied by either $\sin(2\pi f_m t)$ or $\cos(2\pi f_m t)$ and the two results are integrated over an integration window, T:

$$I_{\text{lock-in}} = \frac{1}{T}\int_0^T \mathrm{d}t\, M(t)\cos(2\pi f_m t)$$
$$Q_{\text{lock-in}} = \frac{1}{T}\int_0^T \mathrm{d}t\, M(t)\sin(2\pi f_m t) \quad (1)$$

The signal S_0 is proportional to $(I^2_{\text{lock-in}} + Q^2_{\text{lock-in}})^{1/2}$. The constant phase φ can be extracted from $\tan(\varphi) = -Q_{\text{lock-in}}/I_{\text{lock-in}}$. Noise spectral components with frequencies far from f_m will be averaged out in the integration. Therefore, by choosing f_m outside the noise bandwidth, the measurement signal-to-noise ratio can be significantly improved.

The main obstacle in realizing quantum lock-in dynamics is finding a quantum analogue to signal multiplication, which is essential for the mix-down process. In a classical apparatus this is achieved using a nonlinear device with an output that is proportional to the instantaneous product of its inputs. Nonlinear dynamics of the wavefunction cannot be introduced directly, owing to the linearity of Schrödinger's equation. Nevertheless, wavefunction dynamics will be proportional to a product of Hamiltonian terms if the total Hamiltonian does not commute with itself at different times. Operator non-commutativity therefore has an important role in the quantum mix-down process.

To show this in more detail, we turn to the case of a two-level quantum probe, with states $|\uparrow\rangle$ and $|\downarrow\rangle$. We assume that the probe is coupled both to a signal, $S(t)$, and noise, $N(t)$, by $H_{\text{int}} = M(t)\hat{\sigma}_z/2$, where $M(t) = S(t) + N(t)$ and $\hat{\sigma}_x$, $\hat{\sigma}_y$ and $\hat{\sigma}_z$ are the Pauli operators. For a lock-in measurement, $S(t)$ is modulated: $S(t) = S_0\cos(2\pi f_m t + \varphi)$. The probe is initialized to $|\psi_0\rangle = (|\uparrow\rangle + |\downarrow\rangle)/\sqrt{2}$. In a Bloch sphere picture, this state is represented by a vector along the x axis. Under H_{int}, the superposition phase (the angle between the Bloch vector and the x axis) is oscillating back and forth as a result of the signal and is randomly varying owing to the effect of noise. To implement a lock-in

[1]Department of Physics of Complex Systems, Weizmann Institute of Science, PO Box 26, Rehovot 76100, Israel.

measurement, we mix the probe phase with an oscillating signal by adding to $H_{\rm int}$ an oscillating term that does not commute with $\hat{\sigma}_z$: $H=(M(t)\hat{\sigma}_z+\Omega(t)\hat{\sigma}_y)/2$. If $\Omega(t)$ is periodic and synchronized with $S(t)$, then the phase accumulated owing to $S(t)$ coherently adds up whereas the random phase accumulated owing to $N(t)$ is averaged away. The probe superposition is characterized by the probability of finding the probe in the $|\uparrow\rangle$ state, $P_\uparrow$, and the superposition relative phase, $\phi_{\text{lock-in}}$. By measuring both at time T, we extract the quantum lock-in signal:

$$\phi_{\text{lock-in}}=\frac{1}{\hbar}\int_0^T \mathrm{d}t\, M(t)\cos\left(\frac{1}{\hbar}\int_0^t \mathrm{d}t'\,\Omega(t')\right)$$
$$1-2P_\uparrow=\frac{1}{\hbar}\int_0^T \mathrm{d}t\, M(t)\sin\left(\frac{1}{\hbar}\int_0^t \mathrm{d}t'\,\Omega(t')\right) \quad (2)$$

Equation (2), where $\hbar$ is Planck's constant divided by 2π, resembles the classical lock-in output in equation (1). Specifically, for a constant $\Omega(t)\equiv\Omega_0$, the lock-in outputs $\phi_{\text{lock-in}}$ and $1-2P_\uparrow$ faithfully represent the two signal quadratures. Here, instead of reading out a classical parameter, the quantum lock-in read-out requires repetitive quantum projection measurements. We note that the two signal components can be interchanged through single quantum bit rotations. A full derivation and discussion of equation (2) can be found in Supplementary Information.

In our experiment, we use the two spin states of the electronic ground level of a single $^{88}Sr^+$ ion, $|\uparrow\rangle=|5s_{1/2},\,J=1/2,\,M_J=1/2\rangle$ and $|\downarrow\rangle=|5s_{1/2},\ J=1/2,\ M_J=-1/2\rangle$, as a two-level quantum probe (Fig. 1a). Here J is the total electron angular momentum quantum number and M_J is its projection along the magnetic field axis. Set-up details can be found in Supplementary Information. An energy difference of 5.72 MHz between the probe states is determined by an external d.c. magnetic field. We are able to perform all possible spin rotations by pulsing a resonant radio-frequency magnetic field and tuning the pulse duration and the radio-frequency field phase, $\phi_{\rm rf}$. State initialization and measurement are performed by optical pumping and state-selective fluorescence, respectively. Because the probe states are first-order sensitive to magnetic fields, the main noise mechanism is magnetic field noise, with dominant spectral contributions at the 50-Hz line and its harmonics. Examples for signals that we can measure are modulated magnetic or light fields, respectively measured through their resulting Zeeman or light shifts.

The lock-in sequence is depicted in Fig. 1b. Following optical pumping, a $\pi/2$ rotation initializes the ion probe to $|\psi_0\rangle=(|\uparrow\rangle+|\downarrow\rangle)/\sqrt{2}$. To modulate the ion probe, we apply a train of N π pulses, equally spaced $\tau_{\rm arm}$ apart. Here, ideally $\Omega(t)=\sum_{n=1}^{N}\delta(t-n\tau)\pi$, where $\delta(t)$ is the Dirac delta function. Therefore, the cosine term in equation (2) is a square waveform with a period of $2\tau_{\rm arm}$ and the sine term vanishes. Consequently, a measured signal has to be modulated at $f_{\rm m}=1/2\tau_{\rm arm}$ and in phase with the ion modulation, that is, $\varphi=0$. Here $\phi_{\text{lock-in}}$ is proportional to the signal magnitude, S_0. To measure the probe phase, we complete the sequence with an additional $\pi/2$ rotation, with a relative $\phi_{\rm rf}$ phase with respect to the initial $\pi/2$ pulse. We then detect the probability of the ion being in the $|\uparrow\rangle$ state, $P_\uparrow=1/2+(A/2)\cos(\phi_{\rm rf}-\phi_{\text{lock-in}})$. By scanning $\phi_{\rm rf}$, we are able to retrieve both $\phi_{\text{lock-in}}$ and the cosine fringe contrast, A, using a fitting procedure.

Ideally $A=1$. In practice, noise processes decrease A. As seen from equation (2), even in the absence of any signal, $N(t)$ will contribute a lock-in phase of

$$\phi_N=\frac{1}{\hbar}\int_0^T \mathrm{d}t\, N(t)\cos\left(\frac{1}{\hbar}\int_0^t \mathrm{d}t'\,\Omega(t')\right)$$

The cosine fringe is therefore reduced in the process of averaging: $A=\langle\cos(\phi_N)\rangle$, where angle brackets denote an average over different noise realizations.

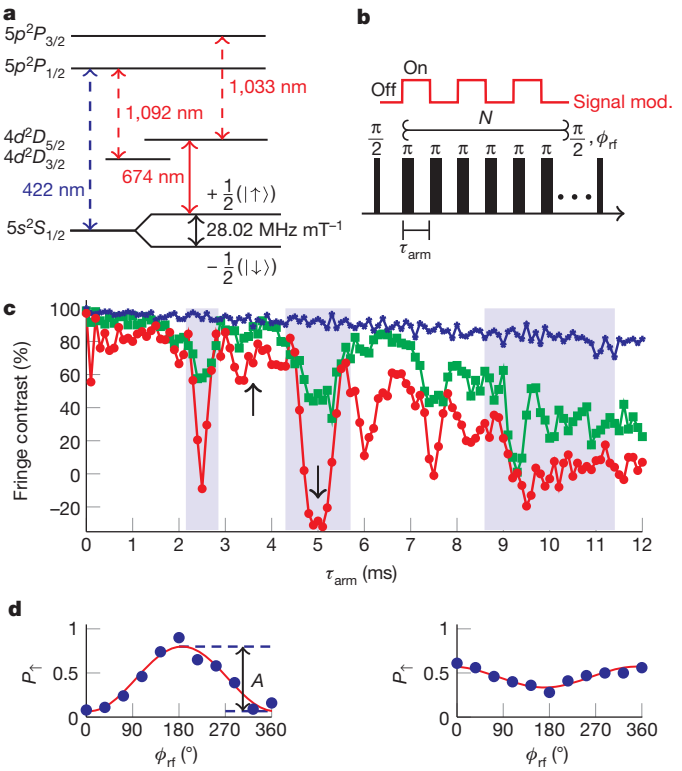

Figure 1 | Measurement scheme. **a**, Level diagram of a $^{88}Sr^+$ ion. The probe spin states are $|\uparrow\rangle=|5s_{1/2},\,J=1/2,\,M_J=+1/2\rangle$ and $|\downarrow\rangle=|5s_{1/2},\,J=1/2,\,M_J=-1/2\rangle$. An external magnetic field splits the two levels by a frequency of $f_0=5.72$ MHz. Spin rotations are performed using an oscillating magnetic field. Initialization to $|\uparrow\rangle$ is done by optical pumping. Spin detection is performed by shelving the $|\uparrow\rangle$ state to the metastable level $|D\rangle\equiv|4d_{5/2},\,J=5/2,\,M_J=+3/2\rangle$, with a narrow-linewidth (<100-Hz), 674-nm laser, followed by state-selective fluorescence at 422 nm. The 1,092-nm and 1,033-nm lasers are used as repump lasers. **b**, The quantum lock-in measurement pulse scheme. The ion is initialized to $(|\uparrow\rangle+|\downarrow\rangle)/\sqrt{2}$ by a $\pi/2$ pulse. While the measured signal is modulated, the superposition is also modulated, in phase with the signal, by a train of N π pulses, $\tau_{\rm arm}$ apart. The total relative phase, $\phi_{\text{lock-in}}$, of the ion superposition, $(|\downarrow\rangle+e^{i\phi_{\text{lock-in}}}|\uparrow\rangle)/\sqrt{2}$, accumulated during the lock-in sequence is measured by scanning the phase of a final $\pi/2$ pulse, $\phi_{\rm rf}$, followed by spin detection and a fit of the data to $P_\uparrow=1/2+(A/2)\cos(\phi_{\rm rf}-\phi_{\text{lock-in}})$. **c**, Fringe contrast, A, versus half lock-in modulation period, $\tau_{\rm arm}$, in the absence of any modulated signal. Data corresponding to $N=1$, 9 and 17 π pulses are shown using blue stars, green rectangles and red circles, respectively. We observe contrast drops as $\tau_{\rm arm}$ approaches 2.5, 5 and 10 ms corresponding to magnetic field noise components at 200, 100 and 50 Hz, respectively. **d**, Probability of finding the ion in the $|\uparrow\rangle$ state versus $\phi_{\rm rf}$. Fringe plots for $\tau_{\rm arm}=3.6$ ms (left) and 5 ms (right), made with lock-in sequences of $N=17$ π pulses, are shown. The solid line is a best fit to $P_\uparrow=1/2-(A/2)\cos(\phi_{\rm rf})$. The fitted A values are shown in **c** at the locations indicated by the two black arrows. The inverted sign of the second fringe can be understood in terms of equation (4).

The reduction in the fringe contrast has significant implications for the lock-in measurement sensitivity. The lock-in signal, $\phi_{\text{lock-in}}$, is proportional to the energy shift experienced by the probe and can therefore be expressed in terms of frequency or magnetic field. Equation (2) implies that the conversion factor depends on the actual modulation type being used. This is discussed in Supplementary Information, where we also show that the optimal frequency-shift measurement sensitivity, s, is

$$s=\frac{1}{2\pi}\sqrt{\frac{4-A^2}{2A^2T}}\,\mathrm{Hz\,Hz^{-1/2}} \quad (3)$$

Here $T\equiv(N+1)\tau_{\rm arm}$ is the total sequence duration and N is the number of π pulses. The standard quantum limit on the sensitivity is reached when $A=1$. To optimize sensitivity, the lock-in modulation frequency

and the sequence duration should be chosen so as to minimize the spectral overlap of noise and modulation and therefore maximize A.

We initially quantify the noise floor of our lock-in detector at different modulation frequencies, f_m, and lock-in sequence durations, T, in the absence of any modulated signal. To begin with we perform this measurement at low lock-in modulation frequencies, which are comparable to typical magnetic noise frequencies in our laboratory. We measure A for values of the π-pulse interspacing, τ_{arm}, ranging from 0 to 12 ms, and for $N = 1$–17 π pulses per lock-in sequence. Both the lock-in sensitivity and the spectral resolution increase as N increases. As shown in Fig. 1c, dips in the fringe contrast emerge as we increase N. These dips, marked by shading, correspond to a.c. magnetic field noise components at frequencies of 200, 100 and 50 Hz, respectively. Figure 1d shows two phase scans for an $N = 17$ lock-in sequence. One scan is at $\tau_{arm} = 3.6$ ms, where no noise is present, and the other is at $\tau_{arm} = 5$ ms, where the lock-in modulation has the same period as the 100-Hz noise component.

To use the lock-in method to quantify the magnetic noise spectrum, we assume that it is composed mainly of discrete frequency components, $f_n = \omega_n/2\pi$, with corresponding amplitudes B_n. With this assumption we can calculate

$$A(N,\tau_{arm}) = \prod_n J_0\left(\frac{-4g\mu_B}{\hbar}\frac{B_n}{\omega_n}\sin^2\left(\frac{\omega_n\tau_{arm}}{2}\right)\frac{\sin(N\omega_n\tau_{arm})}{\sin(\omega_n\tau_{arm})}\right) \quad (4)$$

Here J_0 is the zeroth Bessel function of the first kind, g is the Landé g-factor and μ_B is the Bohr magneton. We note that A can have negative values, as demonstrated by the inverted sign of the second scan of Fig. 1d. In Fig. 2a, we show A (filled circles) for a lock-in sequence with $N = 17$ and a best fit to equation (4) (solid line). Here we assume four discrete magnetic noise spectral components with respective frequencies of 50, 100 and 150 Hz and f_{slow}, the last a slowly varying field. The noise amplitudes are taken as fit parameters, yielding $B_{50\,Hz} = 540(3)$ pT, $B_{100\,Hz} = 390(5)$ pT, $B_{150\,Hz} = 260(4)$ pT and $g\mu_B B_{slow} f_{slow}/h = 37(4)$ Hz^2. The relatively low magnetic field amplitudes are due to an active magnetic field noise cancellation system. A detailed report of the findings described in this paragraph is under way (S.K., N.A, Y.G. and R.O., manuscript in preparation).

Observing that noise amplitudes at frequencies of more than 200 Hz are negligible, we turn to higher modulation frequencies, in search of the greatest attainable probe coherence time. We modulate the ion probe at $f_m = 312.5$ Hz ($\tau_{arm} = 1.6$ ms). Figure 2b shows the fringe contrast A versus N, up to $N = 650$. Here, owing to the large number of π pulses, ϕ_{rf} alternates by π/2 between consecutive pulses, to prevent rotation errors from coherently accumulating. A fit to an exponential decrease in fringe contrast yields a probe coherence time of 1.4(2) s. This is three orders of magnitude longer than the coherence time in the absence of lock-in modulation, measured using Ramsey spectroscopy.

From the data presented so far, we can report our probe's best sensitivity. We calculate the lock-in sensitivity versus T, the total lock-in sequence duration, from the fringe contrast, A, using equation (3). Figure 2c shows the lock-in sensitivity in the low modulation frequency range. A minimum of 0.78 Hz Hz$^{-1/2}$ (28 pT Hz$^{-1/2}$) is observed at $T = 120$ ms, between noise components. Figure 2d shows the lock-in sensitivity versus T at $f_m = 312.5$ Hz. Here a best sensitivity of 0.42(3) Hz Hz$^{-1/2}$ (15(1) pT Hz$^{-1/2}$) is observed at the minimum of the fit, with a lock-in sequence duration of $T = 624$ ms. This is, to our knowledge[2,3], the best magnetic field sensitivity reported so far using a single-spin (or pseudo-spin) detector. In both cases, the measured sensitivity differs from the standard quantum limit, shown by the dashed line, by a factor of less than 1.5.

We next demonstrate the lock-in detection of a small signal and experimentally verify equation (2). To this end, we measure the light shift of a narrow-linewidth (<100-Hz) laser nearly resonant with the $|{\uparrow}\rangle \rightarrow |D\rangle \equiv |4d_{5/2},\ J = 5/2,\ M_J = 3/2\rangle$ quadrupole transition at 674 nm. The laser amplitude is switched on and off at a rate $f_L = 500$ Hz. With this scheme, both the lock-in and the laser are square-wave modulated. We apply a lock-in sequence of $N = 99$ π pulses and scan the lock-in modulation frequency. Here the 674-nm laser is detuned by $\Delta = -17$ kHz from resonance (red detuned). A laser Rabi frequency of $2\pi \times 840$ Hz is independently measured by

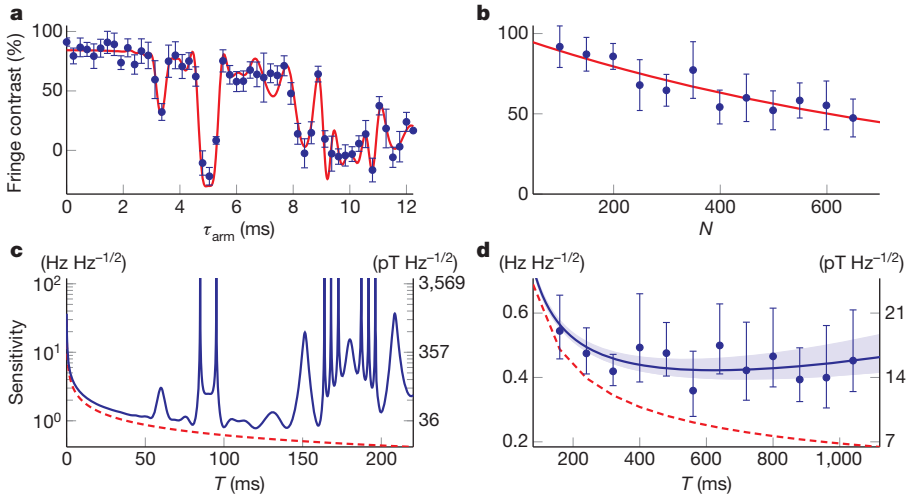

Figure 2 | Sensitivity of the quantum lock-in measurement. **a**, Fringe contrast, A, versus τ_{arm} for $N = 17$ π pulses, in the absence of any modulated signal. Each point is the fitted contrast of a corresponding measured fringe as in Fig. 1; error bars are 95% confidence intervals. The data are used to extract the magnetic noise spectrum. The solid red line is a best fit to equation (4) with four fit parameters: the field amplitudes $B_{50\,Hz} = 540(3)$ pT, $B_{100\,Hz} = 390(5)$ pT and $B_{150\,Hz} = 260(4)$ pT and a slowly varying field $g\mu_B B_{slow} f_{slow}/h = 37(4)$ Hz^2. **b**, Fringe contrast, A, versus number of π pulses, N, at a lock-in modulation frequency of $f_m = 312.5$ Hz; error bars are 95% confidence intervals. The red line is an exponential decay fit to the data yielding a 1/e coherence decay time of 1.4(2) s. **c**, Lock-in sensitivity (solid blue line) versus the lock-in sequence duration, T, calculated from **a** using equation (3). The dashed red line is the standard quantum limit on sensitivity (achieved when $A = 1$). A best sensitivity of 0.78 Hz Hz$^{-1/2}$ (28 pT Hz$^{-1/2}$) is observed at $T = 120$ ms. This sensitivity is only a factor of 1.5 greater than the standard quantum limit. The sensitivity diverges whenever A (shown in **a**) crosses zero. **d**, Exponential decay fit (solid blue curve) shown in **b**, translated to sensitivity using equation (3), as in **c**. The shaded region is a 95% confidence interval for the curve. The dashed red line shows the standard quantum limit on the lock-in sensitivity. The solid blue circles are calculated sensitivities of the measured fringe contrast points in **b**, with 95% confidence intervals. A best sensitivity of 0.42(3) Hz Hz$^{-1/2}$ (15(1) pT Hz$^{-1/2}$) is obtained at the minimum of the solid blue curve ($T = 624$ ms). A similar value of 0.4(1) Hz Hz$^{-1/2}$ (13(3) pT Hz$^{-1/2}$) is observed at $T = 560$ ms.

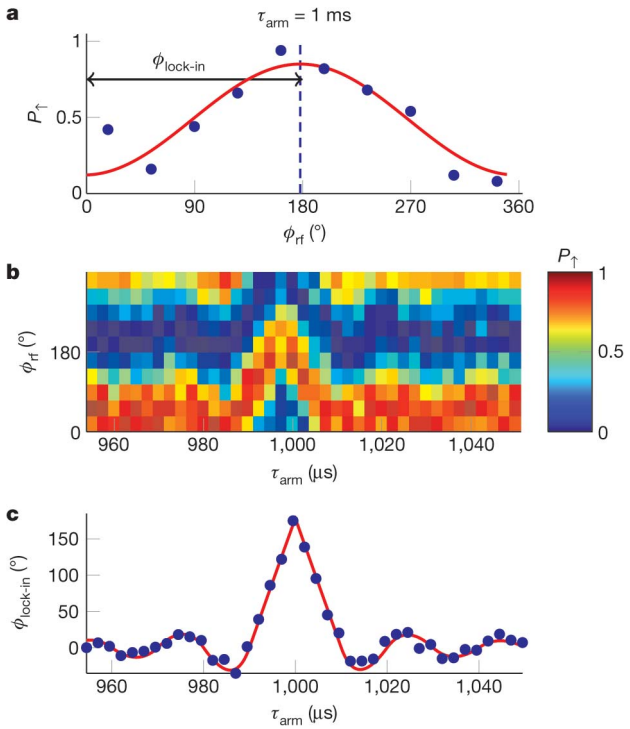

Figure 3 | Lock-in measurement of a small signal. The light shift of the $|\uparrow\rangle$ state induced by the 674-nm laser is measured. The laser is detuned by $\Delta_{674\,nm} = -17$ kHz from the $|\uparrow\rangle \rightarrow |D\rangle$ quadrupole transition, and is amplitude-modulated by a square wave of frequency $f_L = 500$ Hz. The lock-in scheme has $N = 99$ π pulses and the lock-in frequency, $f_m = 1/2\tau_{arm}$, is varied. **a**, Lock-in fringe scan, $P_\uparrow$, versus ϕ_{rf}, at a lock-in period of $2\tau_{arm} = 2$ ms. The red solid line is a best fit to $P_\uparrow = 1/2 + (A/2)\cos(\phi_{rf} - \phi_{lock\text{-}in})$. A clear phase shift of $\phi_{lock\text{-}in} = 0.99\pi$ is observed, with a fringe contrast of $A = 72\%$. **b**, The columns are lock-in fringe scans, similar to that in **a**, for various values of τ_{arm}. The lock-in signal, $\phi_{lock\text{-}in}$, is seen to increase as the lock-in modulation frequency, f_m, approaches the laser modulation frequency, $f_L = 500$ Hz. **c**, Lock-in signal, $\phi_{lock\text{-}in}$, versus τ_{arm}, extracted from **b** as explained in **a**. A light shift of 9.7(4) Hz is measured (with 95% confidence). The solid red line is calculated using equation (2) without any fit parameters.

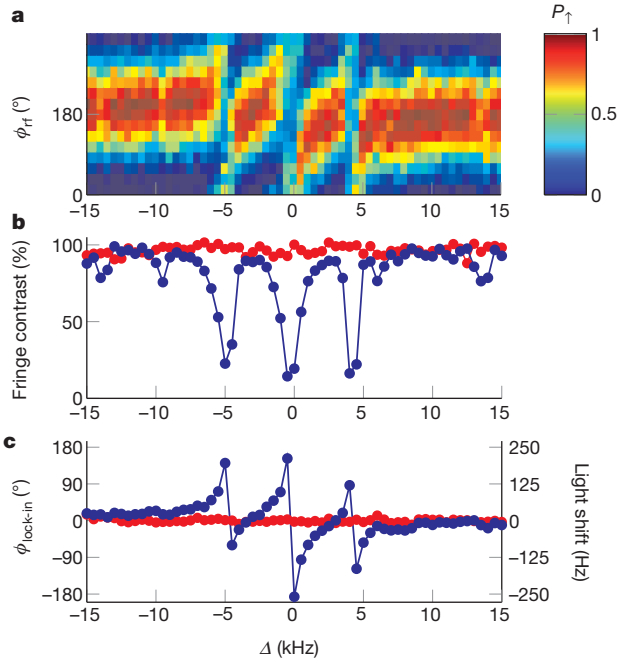

Figure 4 | Light shift spectroscopy. Light shift of $|\uparrow\rangle$ induced by the 674-nm laser, as a function of laser frequency detuning, Δ. At each Δ value, a lock-in sequence of $N = 39$ π pulses with a lock-in period of $2\tau_{arm} = 200$ μs is applied while the 674-nm laser is amplitude-modulated at the same frequency. **a**, Every column is a lock-in fringe scan for a particular value of Δ. For each column, the lock-in signal, $\phi_{lock\text{-}in}$, is the shift of the fringe minimum from zero. **b**, Fringe contrast, A (blue filled circles), versus Δ. Red filled circles show A in the absence of laser light. We observe a reduction in contrast due to shelving of the $|\uparrow\rangle$ state to the metastable level $|D\rangle$ whenever the laser approaches resonance. **c**, Lock-in signal, $\phi_{lock\text{-}in}$ (blue filled circles), versus Δ. The red filled circles show $\phi_{lock\text{-}in}$ in the absence of laser light. Light shifts are seen to have dispersive resonance. Both **b** and **c** show two sidebands, separated by 5 kHz from the transition carrier, generated by the fast amplitude modulation of the laser.

an on-resonance Rabi nutation curve. Figure 3a shows a fringe scan at a lock-in modulation frequency of $f_m = 500$ Hz. The solid line is a best fit to $P_\uparrow = 1/2 + (A/2)\cos(\phi_{rf} - \phi_{lock\text{-}in})$, with A and $\phi_{lock\text{-}in}$ as fit parameters. A clear phase shift of 0.99π is observed. The columns in Fig. 3b are fringe scans similar to that in Fig. 3a, made at different lock-in modulation frequencies. As seen, the lock-in signal is maximal when the modulation frequency approaches 500 Hz ($\tau_{arm} = 1{,}000$ μs), that is, the modulation rate of the laser. Figure 3c shows that the prediction of equation (2) (solid line, calculated without any fit parameters) is in good agreement with measured values (filled circles) of $\phi_{lock\text{-}in}$ as a function of the lock-in modulation rate. A light shift of 9.7(4) Hz is measured; the theoretically predicted value is 9.9(4) Hz.

Any measurement uncertainty is ultimately limited, at long integration times, by slow systematic drifts. The optimal averaging time can be found by performing an Allan deviation analysis[23]. We obtain a minimal measurement uncertainty of 8(2) mHz (290(70) fT) after 3,720 s of averaging. We perform the same analysis for a light shift measurement, obtaining 0.12(2) Hz after 1,320 s. This uncertainty is most probably limited by slow frequency drifts of the 674-nm laser (see Supplementary Information for Allen plots and more details). The magnetic field generated by the valence electron spin of a single $^{88}Sr^+$ ion will cause a level shift of 52 mHz in a probe ion co-trapped one micrometre away, the measurement of which could be within our experimental reach.

Finally, we show how the lock-in method can be used to perform light shift spectroscopy. We probe the $|\uparrow\rangle \rightarrow |D\rangle$ transition. Figure 4a shows lock-in phase scans (columns) for different laser detunings. Figure 4b and Fig. 4c show the fringe contrast, A, and the lock-in signal, $\phi_{lock\text{-}in}$, respectively. Population transfer to level $|D\rangle$ results in a reduction in A whenever the laser is close to resonance. The measured light shift is seen to be dispersive around resonance. The three resonances, a carrier and two sidebands, are due to the fast amplitude modulation of the laser, reminiscent of the Pound–Drever–Hall signal of a laser scanning across an optical cavity resonance[24]. Such a dispersive signal can be used to lock a narrow-linewidth laser to an atomic clock transition.

The results presented here demonstrate the potency of the quantum lock-in measurement technique, which is readily available for any quantum probe. Specifically, with single trapped-ions the lock-in technique allows high-precision frequency-shift measurements with nanometre-scale spatial resolution (in our set-up, the ion wavefunction extent is 9 nm with ground-state cooling). In addition to the detection of a single electronic spin mentioned above, this would be useful to probe spin-dependent interactions of an ion submerged in a quantum degenerate gas[25,26]. Finally, the quantum lock-in technique can be useful for precision measurements and frequency metrology. As an example, it can be used to measure the very small frequency shifts required for the observation of parity non-conservation in a single trapped ion[4]. Another example is the characterization of systematic errors, such as the quadrupole shift, in ion-based atomic clocks[27]. As a final example, the technique can be used to characterize the noise spectrum of narrow-linewidth lasers with respect to an atomic transition.

Received 24 January; accepted 22 March 2011.

1. Giovannetti, V., Lloyd, S. & Maccone, L. Quantum-enhanced measurements: beating the standard quantum limit. *Science* **306,** 1330–1336 (2004).
2. Degen, C. Nanoscale magnetometry microscopy with single spins. *Nature Nanotechnol.* **3,** 643–644 (2008).
3. Balasubramanian, G. *et al.* Ultralong spin coherence time in isotopically engineered diamond. *Nature Mater.* **8,** 383–387 (2009).
4. Fortson, N. Possibility of measuring parity nonconservation with a single trapped atomic ion. *Phys. Rev. Lett.* **70,** 2383–2386 (1993).
5. Rosenband, T. *et al.* Frequency ratio of Al^+ and Hg^+ single-ion optical clocks; metrology at the 17th decimal place. *Science* **319,** 1808–1812 (2008).
6. Knünz, S. *et al.* Injection locking of a trapped-ion phonon laser. *Phys. Rev. Lett.* **105,** 013004 (2010).
7. Kielpinski, D. *et al.* A decoherence-free quantum memory using trapped ions. *Science* **291,** 1013–1015 (2001).
8. Roos, C. F. *et al.* Bell states of atoms with ultralong lifetimes and their tomographic state analysis. *Phys. Rev. Lett.* **92,** 220402 (2004).
9. Langer, C. *et al.* Long-lived qubit memory using atomic ions. *Phys. Rev. Lett.* **95,** 060502 (2005).
10. Leibfried, D. *et al.* Toward Heisenberg-limited spectroscopy with multiparticle entangled states. *Science* **304,** 1476–1478 (2004).
11. Roos, C. F., Chwalla, M., Kim, K., Riebe, M. & Blatt, R. 'Designer atoms' for quantum metrology. *Nature* **443,** 316–319 (2006).
12. Huelga, S. F. *et al.* Improvement of frequency standards with quantum entanglement. *Phys. Rev. Lett.* **79,** 3865–3868 (1997).
13. André, A., Sørensen, A. S. & Lukin, M. D. Stability of atomic clocks based on entangled atoms. *Phys. Rev. Lett.* **92,** 230801 (2004).
14. Wineland, D. *et al.* Experimental issues in coherent quantum-state manipulation of trapped atomic ions. *J. Res. Natl Inst. Stand. Technol.* **103,** 259–328 (1998).
15. Uys, H., Biercuk, M. J. & Bollinger, J. J. Optimized noise filtration through dynamical decoupling. *Phys. Rev. Lett.* **103,** 040501 (2009).
16. Biercuk, M. J. *et al.* Optimized dynamical decoupling in a model quantum memory. *Nature* **458,** 996–1000 (2009).
17. Gordon, G., Erez, N. & Kurizki, G. Universal dynamical decoherence control of noisy single-and multi-qubit systems. *J. Phys. At. Mol. Opt. Phys.* **40,** S75–S93 (2007).
18. Sagi, Y., Almog, I. & Davidson, N. Process tomography of dynamical decoupling in a dense cold atomic ensemble. *Phys. Rev. Lett.* **105,** 053201 (2010).
19. Maze, J. R. *et al.* Nanoscale magnetic sensing with an individual electronic spin in diamond. *Nature* **455,** 644–648 (2008).
20. Hall, L. T., Hill, C. D., Cole, J. H. & Hollenberg, L. C. L. Ultrasensitive diamond magnetometry using optimal dynamic decoupling. *Phys. Rev. B* **82,** 045208 (2010).
21. Naydenov, B. *et al.* Dynamical decoupling of a single-electron spin at room temperature. *Phys. Rev. B* **83,** 081201(R) (2011).
22. de Lange, G., Ristè, D., Dobrovitski, V. V. & Hanson, R. Single-spin magnetometry with multipulse dynamical decoupling sequences. *Phys. Rev. Lett.* **106,** 080802 (2011).
23. Riley, W. J. *Handbook of Frequency Stability Analysis*. NIST Spec. Publ. 1065 (US Department of Commerce, National Institute of Standards and Technology, 2008).
24. Drever, R. W. P. *et al.* Laser phase and frequency stabilization using an optical resonator. *Appl. Phys. B* **31,** 97–105 (1983).
25. Zipkes, C., Palzer, S., Sias, C. & Koehl, M. A trapped single ion inside a Bose–Einstein condensate. *Nature* **464,** 388–391 (2010).
26. Schmid, S., Härter, A. & Denschlag, J. H. Dynamics of a cold trapped ion in a Bose-Einstein condensate. *Phys. Rev. Lett.* **105,** 133202 (2010).
27. Oskay, W. H., Itano, W. M. & Bergquist, J. C. Measurement of the $^{199}Hg^+$ $5d^96s^2$ $^2D_{5/2}$ electric quadrupole moment and a constraint on the quadrupole shift. *Phys. Rev. Lett.* **94,** 163001 (2005).

Supplementary Information is linked to the online version of the paper at www.nature.com/nature.

Acknowledgements We thank G. Bensky, G. Gordon and G. Kurizki for discussions. We acknowledge the support by the ISF Morasha program, the Crown Photonics Center and the Minerva Foundation.

Author Contributions All authors participated in the building of the experimental apparatus. S.K. led the data-taking effort, with help from N.A. Data analysis and development of the analytic theory were performed by S.K. S.K. and R.O. wrote the manuscript. R.O. designed the experiment and supervised the work. All authors participated in discussions, contributed ideas along the way and edited the manuscript.

Author Information Reprints and permissions information is available at www.nature.com/reprints. The authors declare no competing financial interests. Readers are welcome to comment on the online version of this article at www.nature.com/nature. Correspondence and requests for materials should be addressed to S.K. (shlomi.kotler@weizmann.ac.il).